Nanoscale

Accepted Manuscript

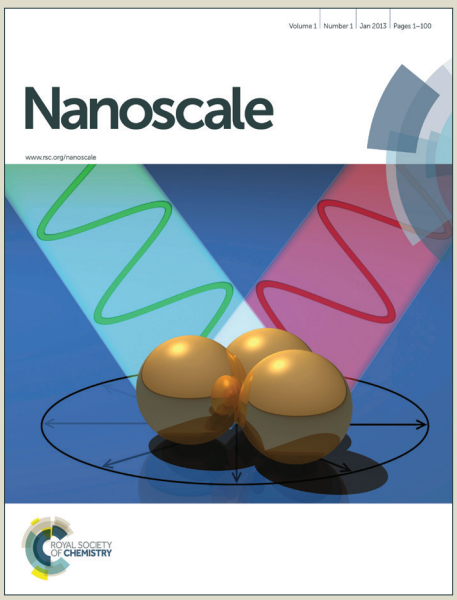

This is an *Accepted Manuscript*, which has been through the Royal Society of Chemistry peer review process and has been accepted for publication.

Accepted Manuscripts are published online shortly after acceptance, before technical editing, formatting and proof reading. Using this free service, authors can make their results available to the community, in citable form, before we publish the edited article. We will replace this *Accepted Manuscript* with the edited and formatted *Advance Article* as soon as it is available.

You can find more information about *Accepted Manuscripts* in the Information for Authors.

Please note that technical editing may introduce minor changes to the text and/or graphics, which may alter content. The journal's standard Terms & Conditions and the Ethical guidelines still apply. In no event shall the Royal Society of Chemistry be held responsible for any errors or omissions in this *Accepted Manuscript* or any consequences arising from the use of any information it contains.

ROYAL SOCIETY OF CHEMISTRY

www.rsc.org/nanoscale

Journal Name

RSCPublishing

ARTICLE

B-doped 3C-SiC nanowires with finned microstructure for efficient visible-light-driven photocatalytic hydrogen production

Cite this: DOI: 10.1039/x0xx00000x

Received 00th January 2012,
Accepted 00th January 2012

DOI: 10.1039/x0xx00000x

www.rsc.org/

Tao Yang,[a] Xiwang Chang,[a] Junhong Chen,[b] Kuo-Chih Chou[a] and Xinmei Hou[a]*

B-doped 3C-SiC nanowires are synthesized via a facile and simple carbothermal reduction method at 1500°C for 2h in flowing purified argon atmosphere. The obtained nanowires possess single crystalline and finned microstructure with fins about 100-200 nm in diameter and 10-20 nm in thickness. While the diameter of the inner core stem is about 80 nm in average. Due to the smaller band gap, the finned microstructure and single crystalline, B-doped 3C-SiC nanowires demonstrate an efficient activity toward H_2 production as high as 108.4 $\mu mol \cdot h^{-1} \cdot g^{-1}$, which is about 20 times higher than that of the 3C-SiC nanowhiskers and 2.6 times of the value reported in the literature.

Introduction

The photocatalytic water splitting over semiconductor photocatalysts to generate hydrogen has attracted increasing attention with sustainable energy and environment emerging as one of the top issues and challenges for humanity.[1–4] Generally the basic mechanism of a photocatalytic reaction is as following[5]: a. the generation and separation of charges after the absorption of light, b. the transmission of charges and c. the reaction between the photo generated charge carriers and solution. It can be seen that charge separation and transfer across interfaces are key aspects in the design of efficient photocatalysts for solar energy conversion. The efficiency of charge separation is determined by the band gap and band structure of the semiconductor. Usually careful design and preparation of structures to maintain the charges being separated and transported efficiently are common methods for the development of photocatalytic materials with improved characteristics. To achieve this goal, many strategies such as noble metal decoration,[6] ion doping,[7,8] structure or morphology modification,[9-12] and combination with other semiconductor photocatalyst[13,14] etc. have been developed. By adopting the above methods, various materials with enhanced photocatalytic activity under visible light irradiation have been developed. For instance, dye-sensitized Au-loaded $SrTiO_3$,[6] nitrogen-doped $La_2Ti_2O_7$ nanosheets,[7] Ni-doped CdS nanowires,[8] necklace-like Ag nanowire-Ag_3PO_4 cube,[9] Cu_2WS_4,[10] C_3N_4,[11] GaN,[12] C_3N_4–MoS_2,[13] Bi_2O_3–Bi_2WO_6[14] and so on. However these photocatalysts are not widely employed owing to their instability or environmentally harmfulness. Therefore considerable efforts are devoted to developing new type of efficient, stable and sustainable visible light-driven photocatalysts.

SiC is an important semiconductor with suitable band gap (2.3-3.3 eV) and excellent properties,[15,16] such as high thermal conductivity, high mechanical strength and high chemical stability, especially the environmentally-friendly property. Therefore SiC can be a promising photocatalyst under visible light irradiation. Wang *et al.* reported that SiC presented a hydrogen evolution ability under visible light.[16] Fujishima *et al.*[17] reported SiC possessed an outstanding reducibility because of its more negative conduction band than other semiconductors, such as TiO_2, CdS, and ZnO. However, SiC as a photocatalyst does not draw wide attention due to the high recombination rate of photo-generated electron-hole pairs as well as its surface evolution during 3C-SiC nanoparticles or nanocrystal contacting with water.[18] To overcome its drawback, some work has been carried out by modifying the microstructure. For instance, Guo *et al.* fabricated modified SiC nanowires as a synergistic catalyst for the hydrogen production reaction.[19] Yuan *et al.* reported SiC coupled with reduced graphene oxide as photocatalysts for enhanced photocatalytic hydrogen production.[20] Dong *et al.* synthesized boron-doped SiC porous structure for visible light driven hydrogen production.[21] However preparation of SiC with high photocatalytic activity using a simple method remains a challenge.

Herein a simple synthesis route combining the ion doping and morphology modification is adopted in the present work. By controlling the amount of boron doping and the reaction temperature, B-doped 3C-SiC nanowires (NWs) with finned microstructure are obtained. It shows an outstanding activity toward H_2 production as high as 108.4 $\mu mol \cdot h^{-1}$, which is about 20 times higher than that of the 3C-SiC nanowires and 2.6 times of the value reported in the literature.

Results and discussion

Effect of B doping amount

The electronic structures of 3C-SiC NWs with different B-doping amount are calculated by plane-wave-density function theory (DFT) using the CASTEP program package. In the calculated models, B atoms is supposed to incorporate into SiC lattice and partly substitute Si sites according to the reported result in the literature.[21,22] The projected density of states (PDOS) of B-doped 3C-SiC with the ratio of B/Si ranging from 0 to 0.143 is shown in Fig.S1. The result shows that 3C-SiC is indirect semi-conductor (Fig. S1a), which is in agreement with the reported reuslt.[22] After B being

Nanoscale Accepted Manuscript

doped, it is changed into direct semiconductor (Figs. S1 b-d). With the molar ratio of B/Si increasing from 0 to 0.143, the band gaps decrease continuously from 2.341eV to 1.935eV as shown in Fig. S1 e. It is well known that the smaller the band gap, the better for hydrogen production. However material with much smaller band gap tends to lead to photo-corrosion. Dong *et al.* [21] synthesized Boron-doped SiC powder for visible light driven hydrogen production. In their work, B-doped 3C-SiC with the B/Si molar ratio of 0.05 exhibits the highest hydrogen evolution rate of 7.41 $\mu mol \cdot g^{-1} \cdot h^{-1}$. Therefore in the experiment, the molar ratio of B/Si is selected as 0.067, i.e. $Si_{15}BC_{16}$.

Characterization of B-doped 3C-SiC NWs

The phase of the B-doped SiC NWs is characterized by X-ray diffraction (XRD) as shown in Fig. S2. For comparison, 3C-SiC NWs obtained in our experiment is also investigated. Three strong diffraction peaks at 2θ =35.8°, 60° and 72° corresponding to the (111), (220) and (311) facets of cubic SiC (JCPDS card no. 73-1665) both appear in the two sample, suggesting B doping does not change the phase structure of 3C-SiC. The detailed magnification of diffraction peak (111) indicates the characteristic peak of B-doped 3C-SiC shifts towards higher 2θ angle. The shift in 2θ values is attributed to the substitution of smaller B (0.095 nm) at Si (0.134 nm) and thus causes the distortion in the crystalline lattice structure.[22] In view of the stacking defects (SF) in B-doped SiC NWs, Tateyama *et al.*[23] studied the stacking defects of SiC and put forward the estimate formula as follows:

$$d_{SF} = \frac{I_{SF}}{I_{(200)}}$$

Where I_{SF} and $I_{(200)}$ are the intensity values of SF peak (about 33.6º) and (200) peak (41.4º), respectively. The ratio value (d_{SF}) represents density of SF in SiC. The larger the index, the more SF the SiC whiskers contained. In this work, the SF and (200) peaks, especially the SF peak marked with red circles in Fig. S2, were too weak to calculate the density of SF by adopting the above equation. On the other hand, indicating that the density of SF in the synthesized SiC whiskers was relatively less.

B-doped 3C-SiC NWs are further characterized using X-ray photoelectron spectroscopy (XPS). The full spectrum of XPS (Fig.1a) shows the existence of Si, C, B. F and O also exist. F possibly comes from HF, which is adopted to treat the surface of sample. In view of O, Si 2p fine XPS spectra of the B-doped 3C-SiC NWs sample are presented in Fig. 1b. From the XPS spectra of Si 2p of B-doped 3C-SiC (Fig.1b), the peak centred at 100.7 eV corresponds to Si-C bond in SiC. The peak at 101.8 eV can be assigned to SiOxCy.[24] Two reasons are attributed to the formation of SiOxCy. First is the surface of sample tends to absorb oxygen after treated by HF. Second is SiCxOy as the intermediate product of SiC[24] is left in the sample. However the content of SiOxCy is too low to be detected by XRD analysis. B 1s fine XPS spectra of the B-doped 3C-SiC NWs sample is shown in Fig. 1c. XPS signals of B 1s are observed at binding energies at around 189.8 eV (B 1s), which can be assigned to the B-C bond in SiC.24 It should be noted that no peaks are found around 187.4 and 193.1 eV, which corresponds to the B-Si bond in SiC and B-O bond for B_2O_3.[25] This indicates that B atoms incorporate into SiC lattice and substitute Si sites, which is in consistent with the reported results.[21,22] The B/Si molar ratio of as determined by XPS is 0.066, which is close to the theoretical content of $Si_{15}BC_{16}$. To further investigate the existence of B element in B-doped 3C-SiC, electron energy loss spectroscopy (EELS) was carried out. The peak centred at 188 eV corresponds to B element. And the peak at 284 eV corresponds to C element (Fig.1d). This further indicates that B-doped 3C-SiC is synthesized in the experiment.

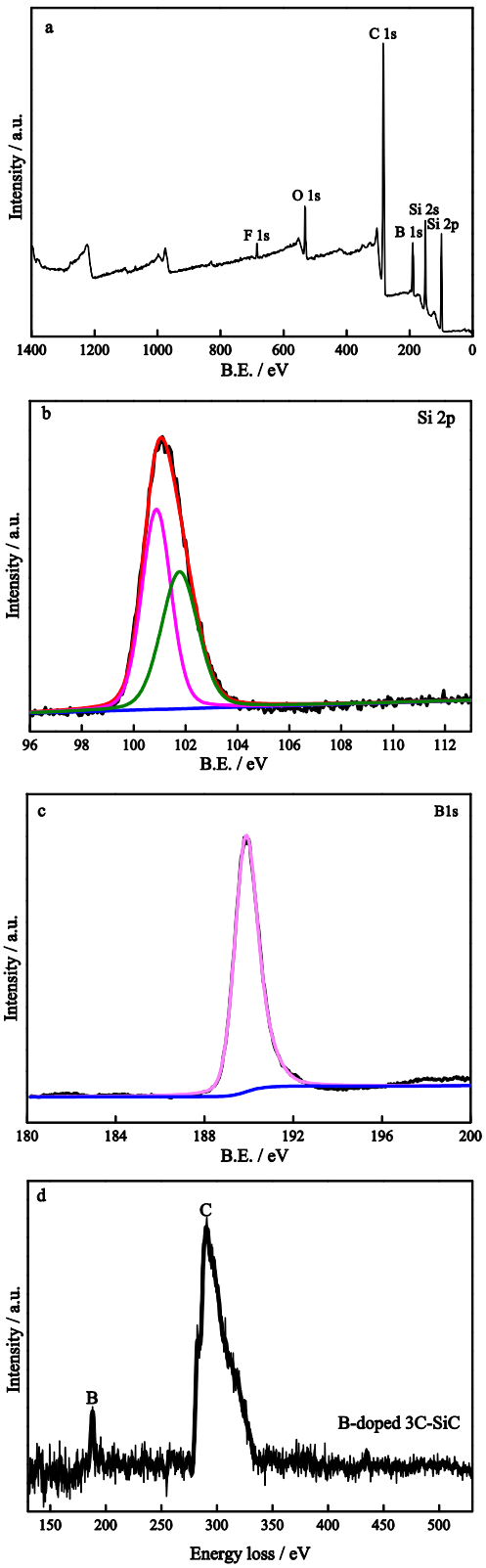

Fig. 1 The full spectrum of XPS of B-doped 3C-SiC (a), XPS spectra of (b) Si 2p, (c) B 1s, (d) Electron energy loss spectroscopy (EELS) of B-doped 3C-SiC.

Nanoscale Accepted Manuscript

This journal is © The Royal Society of Chemistry 2015

The morphology and microstructure of the as-prepared samples are revealed by SEM and TEM techniques. SEM images of the synthesized 3C-SiC NWs are also shown in Fig. 2. The overall looks of the 3C-SiC NWs and B-doped 3C-SiC NWs at low magnification (Fig. 2a and d) indicate the majority of the nanowires can be described as long and straight filaments with the length up to several mm. SEM at higher magnification (Fig. 2b) shows the typical morphology of 3C-SiC NWs possess smooth surface and the average diameter is about 80 nm. With the help of the HRTEM image and the SAED pattern in Fig. 3b, the whisker has a homogeneous crystalline structure with fringes spacing at 2.51Å, which is characteristic of 3C-SiC. By comparison, the morphology of B-doped 3C-SiC NWs changes a lot. The magnified images (Fig. 2e and f) show that the typical morphology of the B-doped 3C-SiC NWs is finned nanowires. It is composed of inner core stems and outer fins. TEM images of typical finned like B-doped 3C-SiC NWs are shown in Fig. 3c and d. The diameter of the fins is about 100-200 nm and the diameter of the inner core stems is about 80 nm. The thickness of the fins is 10-20 nm. The HRTEM image (Fig. 3e) reveals that the lattice spacing of a fin is 2.50 Å. The corresponding SAED pattern inset Fig. 3e shows the nature of the fin on the nanowire is single crystal. In Fig. 3f, the HRTEM image reveals that the lattice spacing of the nanowire is also 2.50 Å. It is caused by substitution of smaller B (0.095 nm) at Si (0.134 nm) and leads to the distortion of lattice.

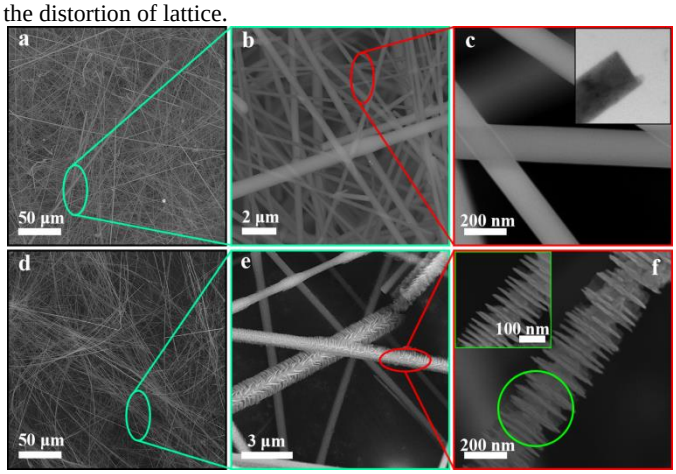

Fig. 2 SEM images of the as-prepared 3C-SiC (a-c) and B-doped 3C-SiC (b-d)

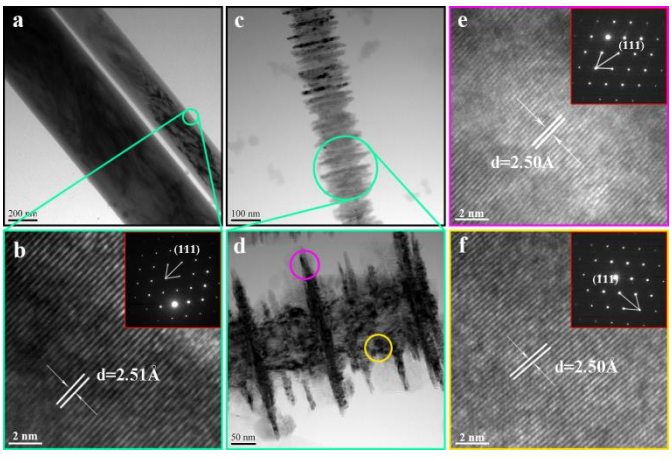

Fig. 3 TEM images of the as-prepared 3C-SiC (a-b) and B-doped 3C-SiC (c-f)

There exist two kinds of growth mechanisms for the formation of hierarchical nanostructures in the literature [26-28]. One is the formation of inner 1D core structures and then the epitaxial growth of secondary branches.[26,27] The other is the self-assembly of nanobuilding blocks, such as platelets, into hierarchical structures.[28] In our experiment, another kind of SiC NWs in small amount is also found, which possesses rough and uneven surface without finned structure (Fig. 4a). Therefore a two-step epitaxial growth process is proposed for finned 3C-SiC NWs (see Fig. 4b). In additon no liquid droplet is found on the tip of the nanowires (the inset of Fig. 2c), indicating the reaction mechanism belongs to the chemical vapor reaction (VS).

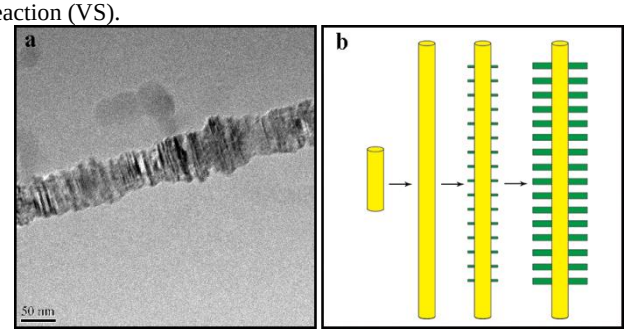

Fig 4. (a). The rough and uneven surface of SiC core stem caused by the stacking faults, (b). Schematic illustration of a possible SiC nanoarchtecture growth process.

In the experiment, the possible reactions take place as following:

$$SiO_2(s) + C(s) \rightarrow SiO(g) + CO(g) \quad (1)$$

$$B_2O_3(g) \rightarrow 2B(s) + 3/2O_2(g) \quad (2)$$

$$15SiO(g) + B(s) + 47CO(g) \rightarrow Si_{15}BC_{16}(s) + 31CO_2(g) \quad (3)$$

$$C(s) + CO_2(g) \rightarrow 2CO(g) \quad (4)$$

SiO vapor is an important intermediate reactant during the synthesis of 3C-SiC whiskers, which is demonstrated in our recent work[29]. The formation of B according to Eq. (2) makes B doping possible and thus is a key step. The standard reaction Gibbs energies of Eq. (2) are 767412.5 J·mol^{-1} using the database of FactSage 6.4.[30] In our experiment, the partial pressure of O_2 is controlled to be 2.6×10^{-12} Pa, which is verified by mass spectrometry. The vapor pressure of B_2O_3 is 152 Pa at 1500°C according to the Speiser's[31] result as following:

$$\lg p_{B_2O_3}\,(\text{atm.}) = -\,(77600/4.575T) + 6.742$$

Therefore, the reaction Gibbs energy of Eq. (2) can be calculated as follows:

$$\Delta rG_{1773} = \Delta rG^{\theta} + RTlnJ$$

$$= 767412.5 + 8.314 \times 1773 \ln \frac{P_{O_2}^{\frac{3}{2}}}{P_{B_2O_3}}$$

$$= 767412.5 + 8.314 \times 1773 \ln \frac{(2.57\times10^{-17})^{\frac{3}{2}}}{1.52\times10^{-3}}$$

$$= -58715.5 \text{ J·mol}^{-1}$$

where J is the reaction constant of Eq. (2) at 1500 °C. Therefore the reaction Gibbs energy of Eq.(2) is calculated to be -58.8 kJ/mol, indicating the reaction can take place under the experimental condition.

During the two-step epitaxial growth process, the first step is the formation of inner 1D core stem owing to the high temperature (1500 °C). Since Eqs. (1) and (2) take place continuously, the reaction between SiO, B and CO occurs to form B-doped SiC($Si_{15}BC_{16}$) (Eq. (3)). CO_2 reacts with C to form CO according to Eq. 4, which causes CO to remain at a supersaturated level and thus Eq. 3 continues to proceed. This leads B-doped SiC($Si_{15}BC_{16}$) to precipitate as nuclei and grow along the [111] direction due to the lowest surface energy to form the core stem B-doped SiC($Si_{15}BC_{16}$) nanowires. Since SiC NWs have more defects after B doping, the nanowires possess rough and uneven surface (as shown in Fig. 4a).

Nanoscale Accepted Manuscript

After holding a certain time, the temperature is decreased and the amount of SiO becomes less. Thus the growth rate of B-doped SiC becomes lower. The newly formed B-doped SiC tends to grow on the protrudes of B-doped SiC core stems because the energy for nucleating SiC on these protrudes is far lower than that on the other places. Therefore, the fins are formed on the core stems. With time prolonging, B-doped SiC nanowire with finned structure are produced.

Water splitting for hydrogen

The 3C-SiC NWs and B-doped 3C-SiC NWs are evaluated under visible-light irradiation for their photocatalytic activities for H_2-production in aqueous suspensions with Na_2S and Na_2SO_3 as sacrificial agents (electron donor). As shown in Fig. 5, photocatalytic activities of B-doped SiC with different B/Si ratios are compared. It can be seen that B doping significantly affects the photocatalytic activity. The photocatalytic H_2-production rate of sample from high to low is $Si_{15}BC_{16}$ (108.4 $\mu mol \cdot h^{-1} \cdot g^{-1}$), Si_7BC_8 (81.0 $\mu mol \cdot h^{-1} \cdot g^{-1}$), $Si_{31}BC_{32}$ (62.1 $\mu mol \cdot h^{-1} \cdot g^{-1}$) and pure 3C-SiC (5.46 $\mu mol \cdot h^{-1} \cdot g^{-1}$). The stability tests are also investigated by carrying out recycling reactions three times for photocatalytic hydrogen production using 3C-SiC NWs and B-doped 3C-SiC NWs ($Si_{15}BC_{16}$) under visible light irradiation. No decrease in catalytic activity is observed in the recycling reactions as shown in Fig. 5b. The H_2 production rate for the B-doped 3C-SiC NWs exceeds that of 3C-SiC NWs by more than 20 times. It also exhibits enhanced activity toward H_2 production compared with the recent work as shown in Fig. 5c. The reported SiC fine powder by Wang's work group can achieved at a value of 1.11 $\mu mol \cdot h^{-1} \cdot g^{-1}$.[32] The reported modified SiC nanowires by Guo's work group can achieved at a value of 2.68 $\mu mol \cdot h^{-1} \cdot g^{-1}$.[19] And the reported boron-doped SiC powder by Dong's work group can achieved at a value of 7.41 $\mu mol \cdot h^{-1} \cdot g^{-1}$.[21] Among these work, the reduced grapheme oxide/SiC showed the larger visible-light-driven photocatalytic hydrogen production done by Yuan's work group to be 42.4 $\mu mol \cdot h^{-1} \cdot g^{-1}$.[20] Our result is 108.4 $\mu mol \cdot h^{-1} \cdot g^{-1}$, which is 2.6 times higher than that of the reported reduced grapheme oxide/SiC.

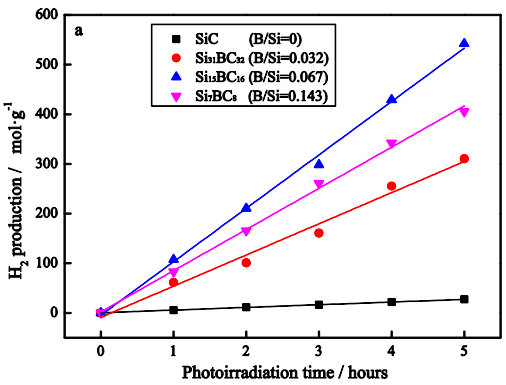

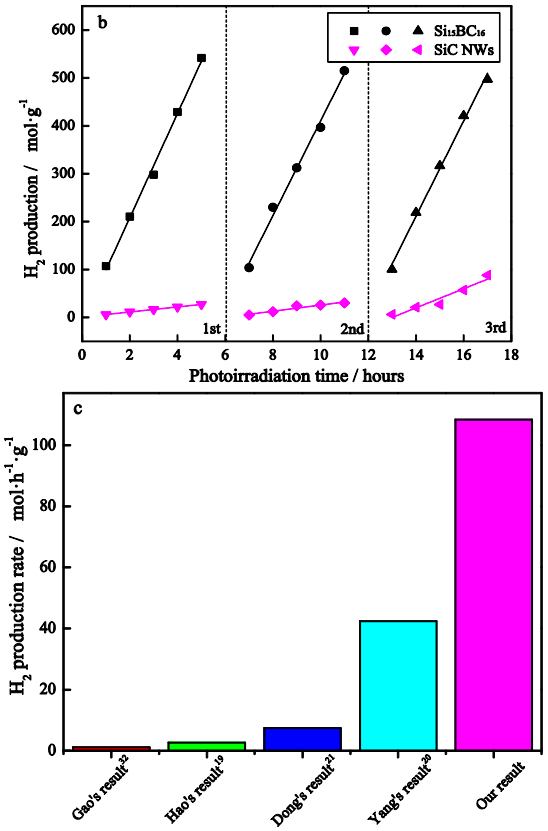

Fig. 5. a. Photocatalytic hydrogen evolution performance over BxSiC, b. Hydrogen production rates of as-prepared the 3C-SiC NWs and B-doped 3C-SiC NWs, b. The comparison of Hydrogen production rates.

In view of the photocatalytic hydrogen production mechanism of B-doped 3C-SiC NWs, first is attributed to the smaller band gaps with B doping as shown in Fig. S1. Since the positions of the valence band maximum (VBM) and the conduction band minimum (CBM) are critical variables in determining the feasibility of efficient visible-light-driven photocatalytic hydrogen production, the partial density of states calculated are shown in Fig. S3. It can be seen that the CB and VB potentials (E_{CB} and E_{VB}) of 3C-SiC are E_{CB}=0 eV and E_{VB}= 2.341 eV (Figs. S3a and b). After B doping, the CB and VB potentials (E_{CB} and E_{VB}) are decreased to E_{CB}=-0.4 eV and E_{VB}= 1.827 eV (Figs. S3c and d). The decrease in CBM of B-doping 3C-SiC is due to the mixing of Si 3p and B 2p orbital and the decrease in the VBM of B-doping 3C-SiC is due to the mixing of C 2s, Si 3s and B 2p orbital. As a result, the CB edge potential of B-doped 3C-SiC is more negative than normal hydrogen electrode (NHE), indicating that under visible-light irradiation photoinduced electrons from the B-doped 3C-SiC can easily transfer from B-doped 3C-SiC NWs to H^+ and generate hydrogen. This can also be confirmed by the UV-vis diffusion reflectance spectra (Fig.S4a). The black line of Fig. S4a is the UV-vis spectra of 3C-SiC NWs, which shows a strong ultraviolet absorption from 200 to 500 nm. After B-doped, the absorption edge extends to the visible region (about 800 nm) (the red line of Fig. S4a) and the absorption intensity is also enhanced. The Kubelka-Munk function is employed to precisely calculate the band gap of the SiC samples.[33] Fig. S4b shows $(\alpha h\nu)^{1/2}$ *versus* E plot for an indirect transition of 3C-SiC NWs and B-doped 3C-SiC NWs. It is obvious that the 3C-SiC NWs (the black line of Fig. S4b) have an intercept value of 2.34 eV, which is close to that of the bulk 3C-SiC (2.35 eV). After B doping, the intercept value is decreased to 2.216

Nanoscale Accepted Manuscript

This journal is © The Royal Society of Chemistry 2015

eV with B doping (the red line of Fig. S4b), which is similar to the calculated value using DFT.

During the photocatalytic process, the photo generated electron recombination is mainly responsible for the low photocatalysis efficiency. Thus this system is expected to effectively suppress electron recombination and leave more charge carriers to form reactive species to facilitate the photocatalytic hydrogen generation. PL quenching effect is an efficient method to determine charge transfer effect within the sample. As shown in Fig. S5, it is observed that the PL intensity of 3C-SiC decreases after B doping. The main reason is that electron is transferred instead of transitions to lower energy level to couple photo which leads to the occurrence of PL. Besides the above reasons, the enhanced electron transfer is also attributed to the special finned like single crystalline nanowires and less stacking defects (as shown in Fig.S2a). This makes the charge pathway much smoother. The special finned like morphology also contributes the higher photocatalytic hydrogen production. This may result from the multiple light reflections within the fins of nanowires (inset Fig. S6) and increase the contacting area with aqueous suspensions.

Conclusion

B-doped 3C-SiC NWs with finned nanostructure as photocatalyst were synthesized via a facile and simple carbothermal reduction of a mixture of low-cost gangue, carbon black and boric oxide powder. The finned microstructure of B-doped 3C-SiC NWs is formed through a two-step epitaxial growth process. Combining the theoretical calculation and experimental result, B substitutes Si during the doping process and posses smaller band gaps. B-doped 3C-SiC NWs demonstrates enhanced and stable activity toward H_2 production as high as 108.4 $\mu mol \cdot h^{-1}$, which is about 20 times of that of 3C-SiC and 2.6 times of the value reported in the literature. It appears that the combined effect of such factors as the single crystal, electronic structures and the finned like morphology is attributed to the enhanced photocatalytic hydrogen production. This work presents an applicable method to develop various semiconductors with controllable morphology applied in solar energy conversion, gas sensors and photoluminescence.

Experimental

Preparation of B-doped 3C-SiC nanowires

Gangue, boric oxide, carbon black and hydrofluoric acid were supplied by Sinopharm Chemical Reagent Beijing Co., Ltd (SCRB). Na_2S and Na_2SO_3 were supplied by Aladdin. Argon gas and nitrogen gas was supplied by Haipu Gas Co., Ltd. Deionized water was used in all experiments.

Gangue (SiO_2 > 99%) and carbon black with the mole ratio of 1:3 was ball mixed. Then the resulting mixture and boric oxide powder (≥98%) were put in different ceramic boats respectively and placed in the hot zone of the furnace equipped with carbon as inner lining. The mole ratio of boric oxide, gangue and carbon black was 1:32:96. Before heating, the furnace was vacuumed and then argon with high purity was introduced at a constant gas flow. The pressure was maintained at 1 atm throughout the whole experiment. The furnace was then slowly heated to 1500°C at the heating rate of 3°C/min and kept for 2 h. Then the furnace was cooled to 800°C at the rate of 3°C/min and cooled naturally to room temperature. During the whole heating and cooling stages, argon was used as protecting atmosphere. Finally gray-white whiskers with large scale were obtained. The obtained whiskers were washed with 10% hydrofluoric acid (HF) for 1h to remove the residual silica.

Characterization

The obtained products were characterized with X-ray diffraction (XRD) with Cu Kα radiation (λ= 1.54178 Å) (XRD, TTRIII, Rigaku). The accelerating voltage and the applied current were 40 kV and 40 mA, respectively. Transmission electron microscopy (TEM) and high-resolution transmission electron microscopy (HRTEM) images were collected by using a JEOL model JEM 2010 EX microscope, using an accelerating voltage of 200 kV. The optical properties of the samples were analyzed by UV-Vis diffuse reflectance spectroscopy (UV-Vis DRS) using a UV-Vis spectrophotometer (UV2250, Shimadzu), in which $BaSO_4$ was used as the background. The chemical states of B-doped SiC nanowires samples were determined by X-ray photoelectron spectroscopy (XPS) in a VG Multilab 2009 system (UK) with a monochromatic Al Kα source and charge neutralizer.

Calculations

The first-principle calculations were carried out using plane-wave pseudo-potential with Cambridge Serial Total Energy Package (CASTEP) code. The Broyden–Fletcher–Goldfarb–Shanno (BFGS)[34] method is used to optimize the geometry structure and convergence tolerance quality is chosen to be fine quality, all the calculation conditions are listed in Table S1. The generalized gradient approximation (GGA)[35,36] for the DFT exchange-correlation function was used in the calculation, as specified by Perdew and Wang 91.[37] The electronic minimization method was choosing the density mixing option.[38] The self-consistent field was set to 1×10^{-6} eV/ atom.

SiC is known to have more than 200 polytypes of different crystal structures.[39] 3C-SiC with zinc blende structure is shown in Scheme S1 (a), and its lattice constant is a=b=c=0.4341 nm. The optimized 3C-SiC and B-doped 3C-SiC($Si_{31}BC_{32}$, $Si_{15}BC_{16}$ and Si_7BC_8) simple cubic crystal structures are shown in Fig.S7 (a)-(d), where Si in the symmetrical positions of 3C-SiC crystal cell has been substituted by B.[21,22] There is no difference for the microstructure of B-doping SiC either selecting B atom in the center site or at the four corner sites except that the number of atoms at the edge sites is different. The aim of selecting B atom in the center of the lattice is for a better symmetry and at the same time can save the calculation time. The k-point set mesh parameters are chosen to be fine quality in the Brillouin zone for B-doped 3C-SiC($Si_{31}BC_{32}$, $Si_{15}BC_{16}$ and Si_7BC_8) corresponding to B concentration about 14.3 at%, 6.7 at% and 3.2 at% respectively.

Photocatalytic tests

Photocatalytic hydrogen production was carried out in an air free closed gas circulation system reaction cell made of quartz. The total cylindrical volume of the cell was 200 mL. An optically polished piece of quartz glass was fused on top of the cell to minimize light scattering. Hydrogen evolution was detected using a gas chromatograph (Beijing, GC-3240, TCD, Ar carrier), which was connected to a gas-circulation line. Argon with a flow rate of 100 $mL \cdot min^{-1}$ was used as a carrier gas, and was passed through the quartz glass cell.

In a typical photocatalytic experiment, 0.2 g of the prepared 3C-SiC nanowires and B-doped 3C-SiC nanowires photocatalysts were dispersed under constant stirring in a 200 mL mixed solution of Na_2S (5mL, 0.1 $mol \cdot L^{-1}$), Na_2SO_3 (5 mL, 0.04 $mol \cdot L^{-1}$) and distilled water (190 mL). The reaction was initiated by irradiation with a 300 W xenon lamp fitted with a cutoff filter (λ > 420 nm). The whole system, including the photocatalyst, was flushed with Ar at 100 mL min^{-1} for 1 h to

Nanoscale Accepted Manuscript

remove any trace of air (including nitrogen and oxygen) before any photocatalytic reaction was carried out. During the process, agitation of the solution ensured uniform irradiation of the suspensions. A 0.4 mL sample of the generated gas was collected intermittently through the septum, and hydrogen content was analyzed by a gas chromatograph (GC-14C, Shimadzu, Japan, TCD, nitrogen as a carrier gas and 5 Å molecular sieve column). All glassware was rigorously cleaned and carefully rinsed with distilled water prior to use.

Acknowledgements

The authors express their appreciation to New Century Excellent Talents in University (NECT-12-0779), the Central Universities of no. FRF-TP-14-113A2, FRF-SD-13-006A and Program for Yangtze Scholars and Innovative Research Team in University (IRT1207) for financial support.

Notes and references

[a] State Key Laboratory of Advanced Metallurgy, University of Science and Technology Beijing, Beijing 100083, China
Email: houxinmei@ustb.edu.cn.
[b] School of Material Science and Engineering, University of Science and Technology Beijing, Beijing 100083, China

1 Z. Wang, J. Hou, C. Yang, S. Jiao, K. Huang and H. Zhu, *Energ. Environ. Sci.*, 2013, **6**, 2134-2144.
2 R. M. Navarro Yerga, M. C. Álvarez Galván, F. Del Valle, J. A. Villoria de la Mano and J. L. Fierro, *ChemSusChem*, 2009, **2**, 471-485.
3 D. Ravelli, D. Dondi, M. Fagnoni and A. Albini, *Chem. Soc. Rev.*, 2009, **38**, 1999-2011.
4 X. Chen, S. Shen, L. Guo and S. Mao, *Chem. Rev.*, 2010, **110**, 6503–6570.
5 H. Wang, L. Zhang, Z. Chen, J. Hu, S. Li, Z. Wang, J. Liu and X. Wang, *Chem. Soc. Rev.*, 2014, **43** , 5234-5244.
6 T. Puangpetch, T. Sreethawong and S. Chavadej, *Int. J. Hydrogen. Energ.*, 2010, **35**, 6531-6540.
7 F. Meng, J. Li, Z. Hong, M. Zhi, A. Sakla, C. Xiang and N. Wu, *Catal. Today*, 2013, **199**, 48-52.
8 S. Li, L. Zhang, T. Jiang, L. Chen, Y. Lin, D. Wang and T. Xie, *Chem-Eur. J.*, 2014, **20**, 311-316.
9 Y. Bi, H. Hu, S. Ouyang, Z. Jiao, G. Lu and J. Ye, *J. Mater. Chem.*, 2012, **22**, 14847–14850.
10 D. Jing, M. Liu, Q. Chen and L. Guo, *Int. J. Hydrogen. Energ.*, 2010, **35**, 8521-8527.
11 X. Wang, K. Maeda, X. Chen, K. Takanabe, K. Domen, Y. Hou, X. Fu and M. Antonietti, *J. Am. Chem. Soc.*, 2009, **131**, 1680-1681.
12 D. Wang, A. Pierre, M. G. Kibria, K. Cui, X. Han, K. H. Bevan, H. Guo, S. Paradis, A. R. Hakima and Z. Mi, *Nano. Lett.*, 2011, **11**, 2353-2357.
13 Y. Hou, A. B. Laursen, J. Zhang, G. Zhang, Y. Zhu, X. Wang, S. Dahl and I. Chorkendorff, *Angew. Chem., Int. Ed.*, 2013, **52**, 3621–3625.
14 H. Wang, S. Li, L. Zhang, Z. Chen, J. Hu, R. Zou, K. Xu, G. Song, H. Zhao and J. Yang, *CrystEngComm*, 2013, **15**, 9011–9019
15 J. J. Chen, Y. Pan, W. H. Tang and Q. Shi, *Nano-Micro Lett.*, 2010, **2**, 11-17.
16 F. L. Wang, L. Y. Zhang and Y. F. Zhang, *Nanoscale Res. Lett.*, 2009, **4**, 153-156.
17 T. Inoue, A. Fujishima, S. Konishi and K. Honda, *Nature*, 1979, **277**, 637..
18 C. He, X. Wu, J. Shen and P. K. Chu, *Nano Lett.*, 2012, 12, 1545-1548.
19 J. Y. Hao, Y. Y. Wang, X. L. Tong, G. Q. Jin and X. Y. Guo, *Int. J. Hydrogen. Energ.*, 2012, **37**, 15038-15044.
20 J. Yang, X. Zeng, L. Chen and W. Yuan, *Appl. Phys. Lett.*, 2013, **102,** 083101.
21 L. L. Dong, Y. Y. Wang, X. L. Tong, G. Q. Jin and X. Y. Guo, *Acta Phys-chim. Sin.*, 2014, **30**, 135-140.
22 S. Agathopoulos, *Ceram. Int.*, 2012, **38**, 3309-3315.
23 H. Tateyama; N. Sutoh, and N. Murukawa, *J. Ceram. Soc. Jpn.*, 1988, **96**, 1003-1011.
24 K. Shimoda, J. S. Park, T. Hinoki and A. Kohyama, *Appl. Surf. Sci.*, 2007, **253**, 9450-9456.
25 S. Oswald and H. Wirth, *Surf. Interface. Anal.*, 1999, **27**, 136-141.
26 W. Lu, Y. Ding, Y. Chen, Z. L. Wang and J. Fang, *J. Am. Chem. Soc.*, 2005, **127**, 10112-10116.
27 Y. C. Zhu, Y. Bando and L. W. Yin, *Adv. Mater.*, 2004, **16**, 331-334.
28 L. W. Yin, Y. Bando, Y. C. Zhu, M. S. Li, Y. B. Li and D. Golberg, *Adv. Mater.*, 2005, **17**, 110-114.
29 J. Chen, W. Liu, T. Yang, B. Li, J. Su, X. Hou and K. C. Chou, *Cryst. Growth Des.*, 2014, **14**, 4624-4630.
30 C. W. Bale, P. Chartrand, S. A. Decterov, G. Eriksson, K. Hack, R. B. Mahfoud, J. Melancon, A. D. Pelton and S. Petersen, FactSage, Ecole Polytechnique, Montreal, 2002. http://www.factsage.com/.
31 R. Speiser, S. Naiditch and H. L. Johnston, *J. Am. Chem. Soc.*, 1950, **72**, 2578-2580.
32 Y. Gao, Y. Wang and Y. Wang, *React. Kinet. Catal. L.*, 2007, **91,** 13-19.
33 J. Chen, W. Tang, L. Xin and Q. Shi, *Appl. Phys. A*, 2011, **102**, 213-217.
34 T. H. Fischer and J. Almlof, *J. Phys. Chem.*, 1992, **96**, 9768-9774.
35 D. C. Langreth and M. J. Mehl, *Phys. Rev. B*, 1983, **28**, 1809-1834.
36 A. D. Becke, *Phys. Rev. A*, 1988, **38**, 3098-3100.
37 Y. Wang and J. P. Perdew, *Phys. Rev. B*, 1991, **44**, 13298.
38 G. Kresse and J. Furthmüller, *Phys. Rev. B*, 1996, **54**, 11169-11186.
39 K. B. Park, Y. Ding, J. P. Pelz, P. G. Neudeck and A. J. Trunek, *Appl. Phys. Lett.*, 2006, **89**, 042103-042103-3.

TOC

Nanoscale Accepted Manuscript

 This journal is © The Royal Society of Chemistry 2015

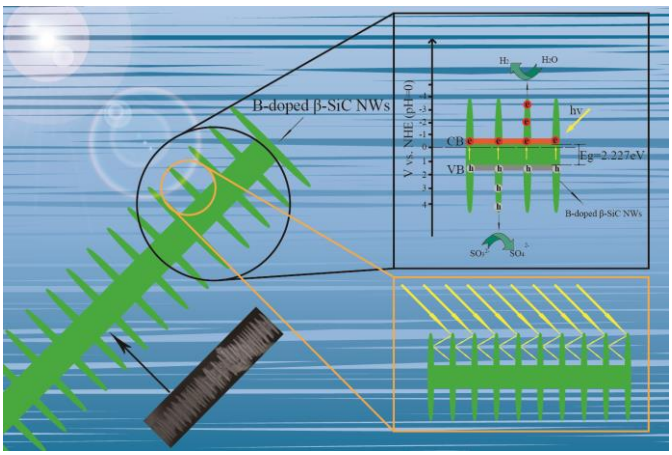

B-doped 3C-SiC nanowires with finned microstructure are synthesized. Due to the smaller band gap, the finned microstructure and single crystalline, B-doped 3C-SiC nanowires demonstrate an efficient activity toward H_2 production as high as 108.4 μmol·h^{-1}·g^{-1}.

Nanoscale Accepted Manuscript